IBRO Neuroscience Reports 17 (2024) 245–251

Contents lists available at ScienceDirect

IBRO Neuroscience Reports

journal homepage: www.sciencedirect.com/journal/IBRO-Neuroscience-Reports

Research paper

Age-related changes of node degree in the multiple-demand network predict fluid intelligence

Lizhi Yu [a,1], Qin Zhang [a,1], Xiaoyang Li [a], Mei Zhang [a], Xiaolin Chen [b], Mingchun Lu [a,*], Zhen Ouyang [a,*]

[a] Department of Radiology, Taian Municipal Hospital, Taian, Shandong, China
[b] Physical examination department, Taian Municipal Hospital, Taian, Shandong, China

ARTICLE INFO

Keywords:
Fluid intelligence
Nodal degree
Multiple-demand network
SMRI
Aging

ABSTRACT

Fluid intelligence is an individual's innate ability to cope with complex situations and is gradually reduced across adults aging. The realization of fluid intelligence requires the simultaneous activity of multiple brain regions and depends on the structural connection of distributed brain regions. Uncovering the structural features of brain connections associated with fluid intelligence decline will provide reference for the development of intervention and treatment programs for cognitive decline. Using structural magnetic resonance imaging data of 454 healthy participants (18–87 years) from the Cam-CAN dataset, we constructed structural similarity network for each participant and calculated the node degree. Spearman correlation analysis showed that age was positively correlated with degree centrality in the cingulate cortex, left insula and subcortical regions, while negatively correlated with that in the orbito-frontal cortex, right middle temporal and precentral regions. Partial least squares (PLS) regression showed that the first PLS components explained 32 % (second PLS component: 20 %, $p_{perm} < 0.001$) of the variance in fluid intelligence. Additionally, the degree centralities of anterior insula, supplementary motor area, prefrontal, orbito-frontal and anterior cingulate cortices, which are critical nodes of the multiple-demand network (MDN), were linked to fluid intelligence. Increased degree centrality in anterior cingulate cortex and left insula partially mediated age-related decline in fluid intelligence. Collectively, these findings suggest that the structural stability of MDN might contribute to the maintenance of fluid intelligence.

Introduction

Fluid intelligence is a physiologically based cognitive ability that reflects an individual's ability to learn and solve problems. Meanwhile, it is arguably the defining feature of human cognition and is associated with a variety of cognitive abilities, such as memory and executive function (Kent, 2017). Fluid intelligence generally declines during normal aging (Michael and Barbey, 2020), affecting the independent living of the older adults. Nevertheless, there are significant individual differences in intelligence, for instance, the parieto-frontal integration theory suggests that the changes in the structure and function of the lateral and medial frontal and parietal lobes and the underlying white matter connections partly explain individual variation in intelligence (Deary et al., 2021). Additionally, cognitive and physical training showcased specific impactions on brain structure and function, which were associated with better intellectual performance (Joubert and Chainay, 2018). Therefore, understanding the brain basis of age-related fluid intelligence decline may help to identify malleable targets that could inform the development of feasible interventions.

In recent years, graph theory analysis has been widely used to reveal the brain structural and functional connectivity patterns related to behavior and cognition, which regards the brain as a network comprising a set of nodes and edges (Liao et al., 2017; Ziegler, 2012). Using graph theory analysis, previous magnetic resonance imaging (MRI) studies have shown age-related alterations in the network properties of large-scale networks, including salience network (SN), fronto-parietal network (FPN) and default mode network (DMN) (Cao et al., 2016; Fan et al., 2021; Malagurski et al., 2020). Using resting-state functional MRI (rs-fMRI) data, Chong et al. found that poorer global cognitive performance in older adults was associated with higher participation coefficient in the control network, Gard found that mindfulness was positively correlated with fluid intelligence and global

* Corresponding authors.
E-mail addresses: xrayflying@163.com (M. Lu), colorfulnerves@163.com (Z. Ouyang).
[1] Contributed equally

https://doi.org/10.1016/j.ibneur.2024.06.005
Received 26 February 2024; Accepted 13 June 2024
Available online 14 June 2024

network efficiency (Chong et al., 2019; Gard et al., 2014). Graph theory analysis of resting state magnetoencephalogram signals also shows that the high frequency functional networks of individuals with high fluid intelligence exhibit lower degree and higher separation (Bruzzone et al., 2022). Graph theory researches have shown that network measures representing different facets of functional architecture are correlated with intelligence, such as clustering coefficients and network efficiency (Li et al., 2009; Zuo et al., 2020). However, little is known about whether age-related alterations in structural network properties can account for the decline in fluid intelligence.

Diffusion-weighted imaging (DTI) is a powerful tool to elucidate local anatomical connectivity, which constructs individual structural networks by tracing the main direction of water molecule diffusion by reconstructing the trajectory of axon bundles.

However, limitations on long-distance projections make it challenging to map the connectivity between all brain regions, and its statistical analysis might be compromised by head movements and false positive connections (Dauguet et al., 2007; Thomas et al., 2014; Walker et al., 2012). Individual structural similarity networks also could be constructed by assessing statistical similarity between brain regions, which might capture biologically meaningful factors associated with development, aging and brain disorders (Wang et al., 2020; Wang et al., 2022). Kong et al. constructed individual structural similarity networks by quantifying the similarity of the probability distribution of gray matter volumes (GMV) in two brain regions, and found that the global and local efficiency of the network decreased with age (Kong et al., 2015). Similarly, compared to healthy controls, Li et al. found that the nodal degree of bilateral superoccipital gyrus and right medial frontal gyrus were smaller in schizophrenia (Li et al., 2019). Wang et al. assessed the reliability of this method for constructing individual structural similarity networks and found that all the network topology properties examined showed fair to excellent reliability, suggesting that single-subject structural network analysis is a reliable method to characterize structural organization of the human brain (Wang et al., 2016).

In the present study, we predict individual fluid intelligence with structural similarity networks, and we hypothesize that age-related changes in hubness of key nodes (nodal degree) would be associated with declines in fluid intelligence. For each participant, we first extracted the GMV of all voxels in each brain region and calculated its probability distribution function (PDF). Second, we quantified the similarity of the probability distribution of GMV in each two brain regions by Kullback–Leibler (KL) divergence and constructed the structural similarity matrix. Third, the similarity matrix was binarized by applying a sparsity threshold. Fourth, we calculated graph-based degree of each node. Finally, node degrees were entered to a partial least squares (PLS) regression model as predictors to predict individual fluid intelligence scores. The main analysis process is shown in Fig. 1.

Methods

Participants

This study included four hundred twenty-two healthy participants (18–87 years old, 199 male and 223 female) from the Cambridge Centre for Ageing and Neuroscience (Cam-CAN, http://www.cam-can.org/) dataset (Supplementary Table 1) (Shafto et al., 2014). Demographic data acquisition, a health and lifestyle questionnaire and Mini-Mental State Exam (MMSE) were conducted for each participant. All participants have high scores (greater than 24) on the MMSE, good hearing (enable to hear 35 dB in either ear), are bilingual English-speakers from birth or native English-speakers, without MRI contraindications and neurological disorders. Written informed consent was obtained from

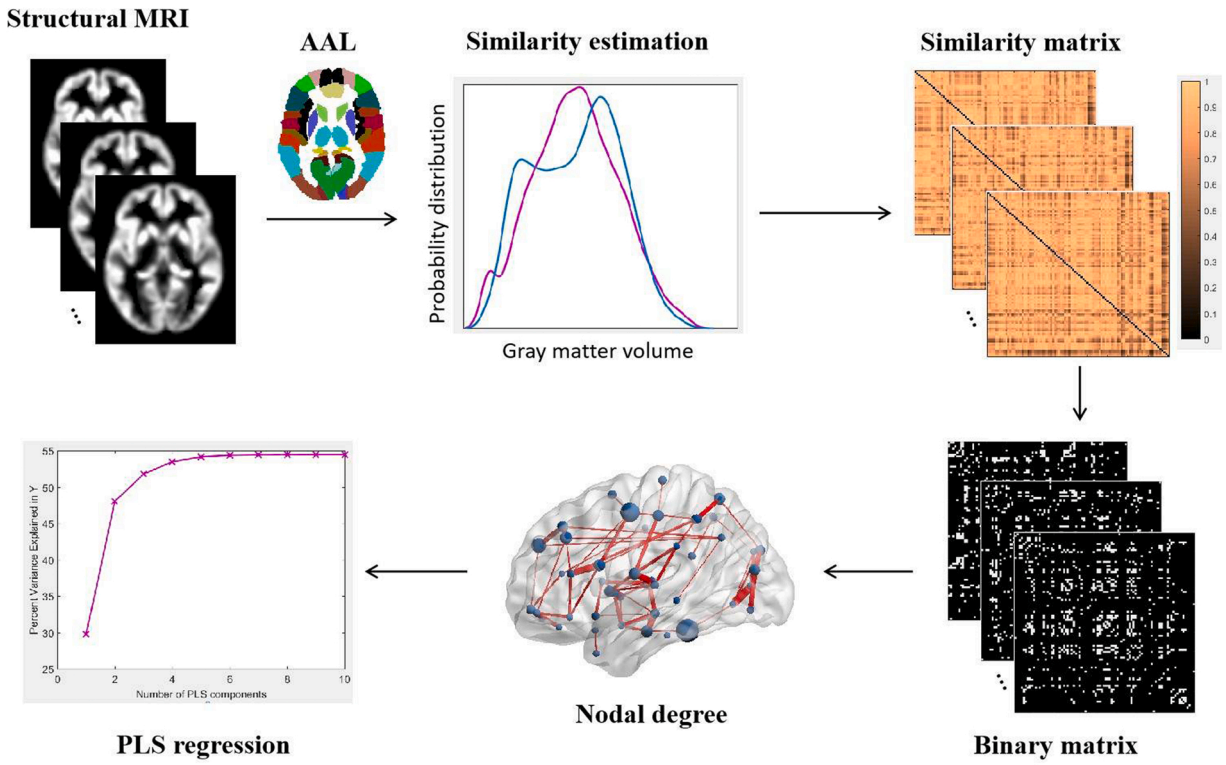

Fig. 1. Analysis flowchart of this study. First, gray matter volume of all voxels in each brain region was extracted from the processed structural magnetic resonance images based on AAL atlas and used to estimate the probability distribution function. Second, KL divergence was used to estimate the similarity of the probability distribution of gray matter volume between each two brain regions, so as to construct the individual similarity matrix. Third, individual binary matrix was created by thresholding the similarity matrix. Fourth, graph-based degree of each node was calculated for each participant. Finally, partial least square regression was performed to predict the individual fluid intelligence score, and node degrees were entered as predictors. MRI, magnetic resonance imaging; AAL, anatomical automatic labeling; KL, Kullback–Leibler; PLS, partial least squares.

each participant, and this study was approved by the Cambridgeshire 2 Research Ethics Committee.

Fluid intelligence test

Fluid intelligence is related to the complex cognitive measures and reflects an individual's ability to respond to complex situations and solve problems (Chen et al., 2020). In this study, fluid intelligence was measured using the standard Cattell Culture Fair, Scale 2 Form A (Shafto, et al., 2014), a pen-and-paper test that contains four subtests (series completion, classification, matrices, conditions) of nonverbal puzzles. Participants chose a response from multiple options and recorded their responses on an answer sheet for each trial. There are 46 trials in total, and a correct response was given a score of 1. Participants with scores below 12 were excluded as not actively participating in the test. In this study, Spearman correlation was performed to examine the relationship between age and fluid intelligence.

Structural MRI images acquisition

All high-resolution (1 mm × 1 mm × 1 mm) 3D T1-weighted images were acquired using a Magnetization Prepared Rapid Gradient Echo (MPRAGE) sequence on a 3 T Siemens TIM Trio System (32-channel head coil). Parameters are as follows: repetition time (TR) = 2250 ms, echo time (TE) = 2.99 ms, inversion time (TI) = 900 ms, field of view (FOV) = 256 mm × 240 mm × 192 mm, flip angle =9 degrees, acceleration factor = 2, acquisition time = 4 minutes and 32 seconds.

Structural MRI images preprocessing

All structural MRI (sMRI) images were preprocessed with the Computation Anatomy Toolbox 12 (CAT12, Department of Psychiatry, University of Jena) to obtain voxel-wise GMV for each participant. First, we examined the structural images of each participant, weeding out those with significant motion artifacts. Second, individual sMRI images were segmented into gray matter (GM), white matter (WM) and cerebrospinal fluid (CSF) using the unified segmentation model with tissue probability maps (TPMs). Third, the GM images were spatially normalized to the Montreal Neurological Institute (MNI) space with a high-dimensional DARTEL algorithm and further nonlinearly modulated to compensate for spatial normalization effects. Fourth, the GM images were resampled to 1.5 mm^3 voxels according to previous study (Wang et al., 2016). Finally, the images were spatially smoothed with a Gaussian kernel of 6 mm full width at half maximum (FWHM). Participants with poor image segmentation and processing quality (below -B) were eliminated. Total intracranial volume (TIV), calculated as the sum of GM, WM, and CSF volumes, was calculated and included as a covariate for further analyses.

Similarity matrix construction

The structural similarity matrix was constructed for each participant using KL divergence, which measures the difference between two probability distributions in probability theory. Specifically, GMV values of all voxels in each brain region were first extracted based on Anatomical Automatic Labeling (AAL) atlas. Then, the probability density functions of GMV in each region were calculated based on a normal kernel function (a MATLAB function: *ksdensity*), and the PDFs were further calculated. Finally, the differences in GMV probability distributions between each of the two brain regions were quantified with KL divergence as follows:

$$D_{KL}(P,Q) = \sum_{i=1}^{n}\left(P(i)\log\frac{P(i)}{Q(i)} + Q(i)\log\frac{Q(i)}{P(i)}\right).$$

P and Q are PDFs of GMV, and n is the number of sample points, 2^7 sampling points were chosen as in previous study (Wang et al., 2016). Since KL divergence is a measure of difference, it was converted to a similarity measure as follows:

$$KLS(P,Q) \quad = e^{-D_{KL}(P,Q)}.$$

e is natural exponential. KL divergence-based similarity (KLS) ranges from 0 to 1, 1 represents identical distributions of GMV between two brain regions. A weighted similarity matrix of an individual is shown in Supplementary Fig. 4 A.

Graph theoretic analysis

The GRETNA toolbox (http://www.nitrc.org/projects/gretna/) was used to perform graph theoretic analysis. Prior to topological characterization of the derived connectivity matrices, a thresholding procedure is typically applied to exclude the confounding effects of spurious connections (Gong et al., 2009). In order to exclude noisy elements, individual structural similarity matrix $C_{ij} = [c_{ij}]$ was converted into a binary network $A_{ij} = [a_{ij}]$ by employing a sparsity threshold S, which was defined as the ratio of the actual number of edges to the maximum possible number of edges in the network:

$$A_{ij} \quad = \quad [a_{ij}] = \begin{cases} 1, \& c_{ij} < KLS_{thres} \\ 0, \& others \end{cases}$$

where KLS_{thres} is subject-specific KLS threshold. With thresholding, there were same number of nodes and edges across all binary networks. Due to the lack of a conclusive method for selecting a single threshold (Lo et al., 2011), a continuous sparsity range of $0.1 < S < 0.7$ (interval = 0.05) was selected following a previous work (Homan et al., 2019). For the brain networks at each sparsity level, the nodal degree was computed for each node, which defined as the number of connections (edges) that a node has with other nodes in the network. As sparsity increases, high-confidence connections are preserved (low-strength or unreliable connections are excluded), and the differences of nodal degree in the network decrease (Lo et al., 2011; Luo et al., 2021). The binarized similarity matrices of an individual at each sparsity level S are shown in Supplementary Fig. 4. Finally, the area under the curve (AUC) of the nodal degree was calculated for further analyses, which reflects the measure across the sparsity parameter S. This method provides a summary scalar for topological characterization and has proven to be sensitive in detecting changes in brain network topology (Li et al., 2021).

Partial least squares regression analysis

First, a multivariable linear regression model was performed to examine the relationship between the nodal degree and age, with gender, education level and TIV as covariates. This model was fitted for each region, and the t-statistic was extracted. Significance was set at $p < 0.05$, and FDR correction was conducted to correct multiple comparisons across all regions. Multivariate PLS regression is used to calculate the optimal low-dimensional solution of the relationship between a set of predictors and response variables, which is suitable for highly collinear predictors and can reduce the risk of overfitting. In the present study, PLS regression was performed to detect the relationship between nodal degree and fluid intelligence. Individual fluid intelligence scores were entered as response variables (422 × 1 vector), the degrees of each node in each participant were entered as predictor variables (422 × 90 matrix). Taking into account the possible effects of inter-individual differences, both the response vector and prediction matrix regressed the effects of potential confounders, including gender (Ingalhalikar et al., 2013), education level (Malagurski et al., 2020) and TIV (Malone et al., 2015). Residuals were used for actual PLS regression analysis. The statistical significance of the variance explained by each PLS component was detected by permuting response variables 5000 times (permutation

test). Spearman correlation coefficients between predictor scores of each PLS component and fluid intelligence were calculated. Bootstrapping was used to estimate the contribution of each node to each PLS component, and the ratio of the weight of each node to its bootstrap standard error was used to calculate the Z scores (Li et al., 2021; Morgan et al., 2019). Normalized Z scores were used to measure the correlation of each node to each PLS component (Homan et al., 2019). To verify the replicability of the results in this study, half of the participants were randomly selected for additional PLS regression analysis. The codes for PLS regression analysis are openly available at https://github.com/SarahMorgan/Morphometric_Similarity_SZ.

Mediation analysis

Further, bootstrapped mediation analysis was performed to investigate whether age-related decline in fluid intelligence was mediated by regional changes of nodal degree. We regressed out the effects of gender, education level and TIV on the independent (X, age), dependent (Y, fluid intelligence) and mediating (M, regional nodal degree). The residuals were normalized and used for further analysis. We examined the relationship between age and regional nodal degree (path a), between the regional nodal degree and fluid intelligence (path b), and the total effect (path c) of age on fluid intelligence. The significance of the indirect effect (path c') of age on fluid intelligence through the regional nodal degree was tested with a bootstrapping analysis (resampled 10,000 times). The mediation analysis was conducted using the Mediation ToolBox (https://github.com/canlab/MediationToolbox).

Results

As shown in Supplementary Fig. 1, we found a significant negative correlation ($r_{420} = -0.58$, $p < 0.001$) between age and fluid intelligence in this study. The first PLS component (PLS1) accounted for 29.78 % of the variance in fluid intelligence, and the explanation rate was significant ($p_{perm} < 0.001$). The PLS1 scores were positively correlated with fluid intelligence ($r_{420} = 0.56$, $p < 0.001$, Fig. 2 A), which indicates the predictive effectiveness of network node degree on individual fluid intelligence. We calculated the ratio of each node's weight to its bootstrap standard error to assess the contribution of each node to PLS1. We found that the nodes with greater weight were mainly located in prefrontal cortex, temporal cortex and middle occipital cortex (Fig. 2 B).

The second PLS component (PLS2) accounted for 19.26 % of the variance in fluid intelligence, and the explanation rate was significant ($p_{perm} < 0.001$). The PLS2 scores were also positively correlated with fluid intelligence ($r_{420} = 0.38$, $p < 0.001$, Fig. 3 A). Meanwhile, the nodes with greater weight were mainly located in posterior cingulate cortex, orbito-frontal cortex, left insula, pallidum and part of precentral regions (Fig. 3 B). As shown in Supplementary Fig. 2, other PLS components were not significantly explain the variance in fluid intelligence ($p_{perm} > 0.05$).

In validation analysis, the second PLS1 and PLS2 accounted for 33.88 % and 27.39 % of the variance in fluid intelligence, respectively (all $p_{perm} < 0.001$). We found significant positive correlation between the PLS1 scores ($r_{209} = 0.59$, $p < 0.001$), PLS2 scores ($r_{209} = 0.45$, $p < 0.001$) and fluid intelligence (Supplementary Fig. 5). Moreover, both PLS1 and PLS2 show a similar spatial distribution pattern of node weights as the discovery analysis ($r_{PLS1} = 0.97$, $r_{PLS2} = 0.88$, all $p_{SMASH} < 0.001$).

For completeness, we also detected the relationship between the nodal degree and age using a multivariable linear regression model, adding gender, education level and TIV as covariates. Confirming previous findings (Chong et al., 2019;Shah et al., 2018), we found increased degree centrality with age in the cingulate cortex, left insula and pallidum, right caudate nucleus and thalamus, and decreased degree centrality with age in the orbito-frontal cortex, right middle temporal and precentral regions (Supplementary Fig. 3 and Supplementary Table 2). Furthermore, we found that increased degree centrality in anterior cingulate cortex, left insula and right caudate nucleus partially mediated the age-related decline in fluid intelligence (Supplementary Fig. 6). Node degree quantifies the number of edges linked to a node and reflects the degree of node participation in information transmission. The decreased node degree indicates that the node's links with other nodes is weakened, and its participation in the network is reduced, while an increase is the opposite. Collectively, these findings showed that nodal degree of several brain regions explain a significant proportion of the variance in fluid intelligence, suggesting that age-related structural similarity network configuration changes might associated with the decline in fluid intelligence.

Discussion

In the present study, to characterize the brain underpinnings for age-related declines in fluid intelligence, we used individual structural similarity networks to predict fluid intelligence. We found increased degree centrality with age in the cingulate cortex, left insula and subcortical regions, and decreased degree centrality in the orbito-frontal cortex, right middle temporal and precentral regions. Additionally, the nodal degrees of the insula and anterior cingulum partially mediated

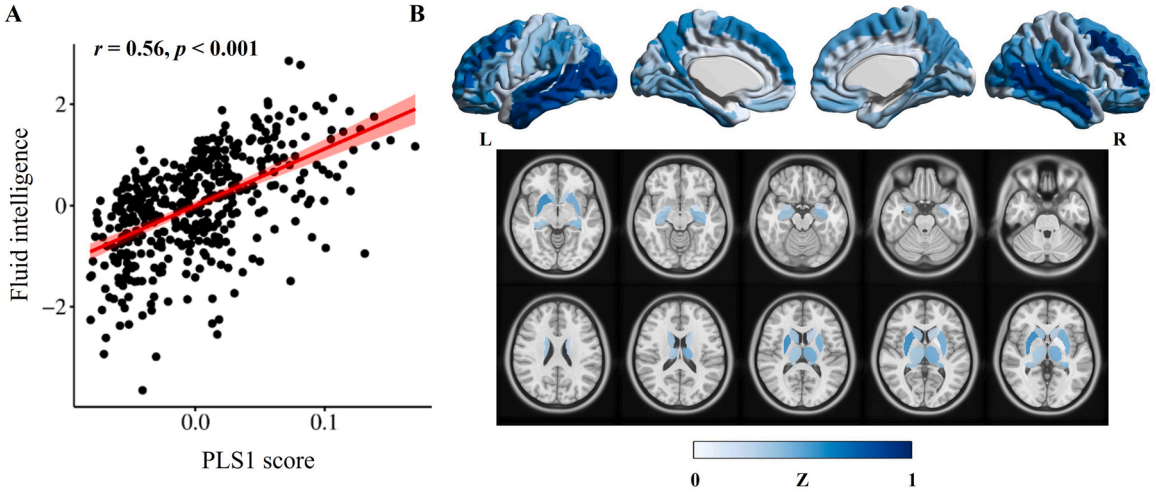

Fig. 2. Correlation between PLS1 scores and individual fluid intelligence scores and contribution of each cortical node. A. The first PLS component was positively correlated with fluid intelligence score (Spearman correlation). B. The weight of each node, i.e. the contribution to the first PLS component.

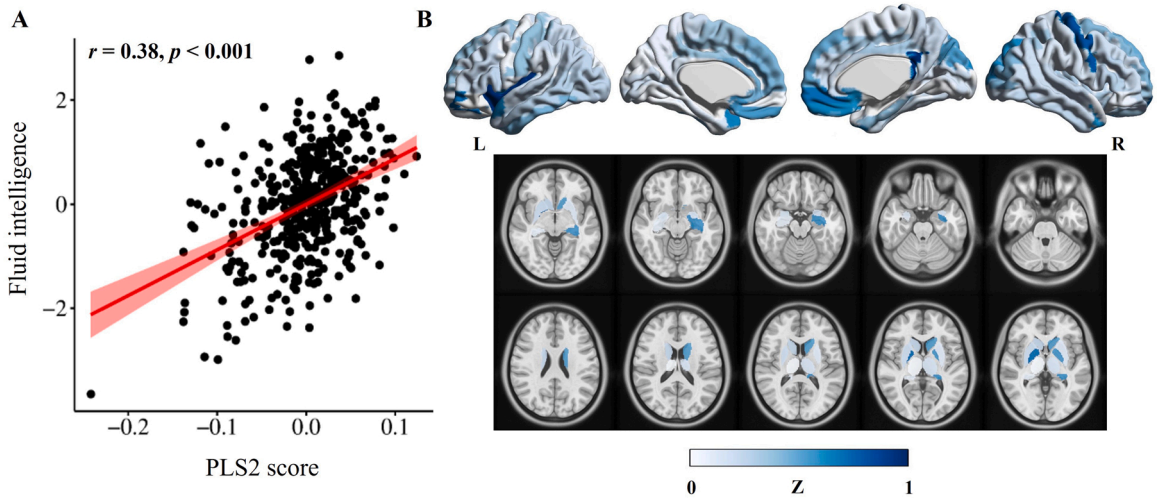

Fig. 3. Correlation between PLS2 scores and individual fluid intelligence scores and contribution of each cortical node. A. The second PLS component was positively correlated with fluid intelligence score (Spearman correlation). B. The weight of each node, i.e. the contribution to the second PLS component.

age-related decline in fluid intelligence. Collectively, this study suggests a link between brain network morphology and individual cognitive abilities, revealing key imaging features of age-related cognitive decline.

The realization of cognitive processes requires the simultaneous activity of multiple brain regions. And the structural similarity network might reflect synchronous changes in distributed cortical regions (Alexander-Bloch et al., 2013). Using sMRI data to construct individual structural similar networks, Li et al. found that morphological networks in patients with major depression accompanied by suicidal ideation showed decreased segregation and weaker integration, as well as abnormal nodal efficiency in fronto-striatum-limbic-thalamic circuit (Li et al., 2021). Kong et al. demonstrated decreased global and local efficiency of structural similar networks across adults aging (Kong et al., 2015). Therefore, structural similarity networks might capture biological signatures associated with development, aging, and neurological diseases. Brain networks contain a minority of hubs, nodes that are highly connected to other regions. We chose nodal degree to predict individual cognitive ability as brain abnormalities associated with cognitive decline should be concentrated in network centers (Liao et al., 2017). Using cross-sectional and longitudinal rs-fMRI data, Chong et al. found that the local efficiency of networks in the elderly was reduced, especially in SN, FPN and DMN (Chong et al., 2019). Older adults exhibit longitudinal reconfiguration of frontoparietal control, default mode, and sensorimotor networks, which might associate with worse processing speed or learning performance (Malagurski et al., 2020). Consistent with these studies, we found that the nodal degree of the prefrontal cortex, orbitofrontal cortex and supplementary motor area was significantly correlated with fluid intelligence, mainly contained in sensorimotor network, FPN and DMN.

Fluid intelligence is associated with multiple-demand network (MDN), which consists of several regions across the frontal and parietal lobes, including middle lateral prefrontal cortex, orbito-frontal cortex, anterior insula, anterior cingulate, supplementary motor area and intraparietal sulcus (Tschentscher et al., 2017). We found that the nodal degree of orbito-frontal cortex and precentral gyrus decreased significantly with age, while the nodal degree of insula and anterior cingulate increased significantly with age, and these changes were associated with the decline of fluid intelligence. Zuo et al. found that the eigenvector centrality in MDN mediated age-related decline in fluid intelligence, supporting the stability of the MDN functional architecture contributes to the maintenance of intelligence (Zuo et al., 2020). Reduced activation in MDN leads to reduced efficiency of fluid intelligence in the older adults (Spreng and Turner, 2019). Cao et al. revealed that increased functional connectivity between lateral prefrontal and superior frontal cortex was associated with better performance after cognitive training (Cao et al., 2016). Better performance of individuals after multi-modal interventions, as reflected by fluid intelligence, can be predicted by larger anterior cingulate cortex volume and smaller middle frontal and insula volumes (Daugherty et al., 2020). Consistent with these findings, we found that changes in the node-degree centrality of MDN are associated with the decline of fluid intelligence, which provides network-based support for the maintenance of intelligence during successful aging (Nyberg and Pudas, 2019; Zuo, et al., 2020).

Additionally, we found age-related changes of nodal degrees in the temporal cortex and some subcortical regions, such as thalamus and putamen, were associated with fluid intelligence. Shah et al. evaluated the effect of age on the topological characteristics of nodes using functional brain networks, found that the nodal degree and efficiency of caudate, pallidum and thalamus were positively correlated with age (Shah et al., 2018). The thalamus acts as a relay station, different thalamic subregions are structurally and functionally connected to a set of cortical regions and thus involved in specific cognitive processes (Parnaudeau et al., 2018;Wolff and Vann, 2019). A recent sMRI study found that putamen volume was a good predictor of intelligence in older adults (Weerasekera et al., 2023). The structure and function of the left temporal lobe are associated with general intelligence. For example, thicker left temporal cortex corresponded to higher general and verbal intelligence quotient scores, which related to the selective adaptation of its cell microstructure and function (Heyer et al., 2022). Overall, the structural integrity and normal function of these regions are essential for the maintenance of fluid intelligence.

In the present study, we constructed morphological brain network by calculating interregional similarity of GMV distribution. Although according to Wang et al., KLS-based morphological similarity networks are specifically organized, analytical strategies sensitive and test–retest reliable, the biological significance underlying the similarity remains unclear (Kong et al., 2014;Wang et al., 2016). One possible explanation comes from axonal extension theory, which suggests that morphologically similar regions are axonally connected to each other (Wei et al., 2019). Moreover, strongly connected regions are cytoarchitectonically similar and have high levels of co-expression genes (Seidlitz et al., 2018). Increasing evidences indicate that the influence of heredity and experience-related plasticity, developmental coordination or synchronous maturation between brain regions, play an important role in the formation of brain morphological networks (Alexander-Bloch et al., 2013;Evans, 2013). Therefore, evaluating developmental, aging or brain disease-related changes in KLS-based brain morphological networks could provide more insights into this speculation in the future.

Limitation

Some limitations of the present study should be mentioned. First, we constructed structural similarity networks by quantifying the similarity of the probability distribution of GMV between each pair of brain regions. Future studies should construct structural similar networks using other structural indicators to further verify the reproducibility of the results, such as cortical thickness and surface area. Meanwhile, further comparisons with other approaches to building structural networks should be made to provide more meaningful insights, such as white matter fiber bundle tracking using DTI. Second, we employed the AAL atlas, a widely used structural atlas in previous structural brain network studies (Kong et al., 2015;Wang et al., 2016), to construct KLS-based structural similarity networks. It is important to provide more comprehensive insights into the effect of different parcellation schemes on the topological organization of individual structural brain networks in the future. Third, we only used node degree as a predictor and did not include other potential prediction data, which means that our findings may not be predictive when other predictors are included in the model. The relationship between other properties of GMV network and age and fluid intelligence should be further demonstrated, such as modularity, network efficiency, etc. Finally, future studies should use longitudinal data and other datasets to reveal age-related changes in structural similar networks and explore their predictive performance for cognitive function.

Conclusion

In conclusion, this study constructed individual structural similarity networks in terms of the KL divergence-based similarity measurement, and further investigated the age-related change pattern and predicted individual fluid intelligence level. The results showed age-related changes of the structural centrality (measured by nodal degree) in the MDN. And the changes of structural centrality were associated with age-related decline in fluid intelligence. This study explores the age-related changes of large-scale brain morphological network topology, which provides a valuable reference for the study of cognitive aging.

Author Statement

We verify that this manuscript is an original work, has not been published elsewhere previously and is not under consideration for publication elsewhere. We additionally verify that all authors provide their approval regarding submission of this manuscript.

All authors declare no competing interests and consent to the publication of the paper.

This study was approved by the Cambridgeshire 2 Research Ethics Committee.

Author Contributions

LMC and OYZ designed the project. YLZ and ZQ analyzed the data and wrote the manuscript. LXY, ZM and CXL contributed to the statistical concepts.

CRediT authorship contribution statement

Mingchun Lu: Project administration, Conceptualization. **Zhen Ouyang:** Writing – review & editing, Project administration. **Mei Zhang:** Investigation. **Xiaolin Chen:** Visualization. **Qin Zhang:** Writing – original draft, Software, Data curation. **Xiaoyang Li:** Validation. **Lizhi Yu:** Writing – original draft, Formal analysis.

Declaration of Competing Interest

All authors declare no competing interests.

Acknowledgments

The authors would like to thank all participants from the Cam-CAN dataset.

Appendix A. Supporting information

Supplementary data associated with this article can be found in the online version at doi:10.1016/j.ibneur.2024.06.005.

References

Alexander-Bloch, A., Giedd, J.N., Bullmore, E., 2013. Imaging structural co-variance between human brain regions. Nat. Rev. Neurosci. 14, 322–336.
Bruzzone, S.E.P., Lumaca, M., Brattico, E., Vuust, P., Kringelbach, M.L., Bonetti, L., 2022. Dissociated brain functional connectivity of fast versus slow frequencies underlying individual differences in fluid intelligence: a DTI and MEG study. Sci. Rep. 12.
Cao, M., Huang, H., Peng, Y., Dong, Q., He, Y., 2016. Toward developmental connectomics of the human brain. Front Neuroanat. 10, 25.
Cao, W., Cao, X., Hou, C., Li, T., Cheng, Y., Jiang, L., Luo, C., Li, C., et al., 2016. Effects of cognitive training on resting-state functional connectivity of default mode, salience, and central executive networks. Front Aging Neurosci. 8, 70.
Chen, P.Y., Chen, C.L., Hsu, Y.C., Cam, C.A.N., Tseng, W.I., 2020. Fluid intelligence is associated with cortical volume and white matter tract integrity within multiple-demand system across adult lifespan. Neuroimage 212, 116576.
Chong, J.S.X., Ng, K.K., Tandi, J., Wang, C., Poh, J.H., Lo, J.C., Chee, M.W.L., Zhou, J.H., 2019. Longitudinal changes in the cerebral cortex functional organization of healthy elderly. J. Neurosci. 39, 5534–5550.
Daugherty, A.M., Sutton, B.P., Hillman, C.H., Kramer, A.F., Cohen, N.J., Barbey, A.K., 2020. Individual differences in the neurobiology of fluid intelligence predict responsiveness to training: evidence from a comprehensive cognitive, mindfulness meditation, and aerobic exercise intervention. Trends Neurosci. Educ. 18.
Dauguet, J., Peled, S., Berezovskii, V., Delzescaux, T., Warfield, S.K., Born, R., Westin, C.-F., 2007. Comparison of fiber tracts derived from in-vivo DTI tractography with 3D histological neural tract tracer reconstruction on a macaque brain. NeuroImage 37, 530–538.
Deary, I.J., Cox, S.R., Hill, W.D., 2021. Genetic variation, brain, and intelligence differences. Mol. Psychiatry 27, 335–353.
Evans, A.C., 2013. Networks of anatomical covariance. NeuroImage 80, 489–504.
Fan, F., Liao, X., Lei, T., Zhao, T., Xia, M., Men, W., Wang, Y., Hu, M., et al., 2021. Development of the default-mode network during childhood and adolescence: A longitudinal resting-state fMRI study. Neuroimage 226, 117581.
Gard, T., Taquet, M., Dixit, R., HÃ¶lzel, B.K., de Montjoye, Y.-A., Brach, N., Salat, D.H., Dickerson, B.C., et al., 2014. Fluid intelligence and brain functional organization in aging yoga and meditation practitioners. Front. Aging Neurosci. 6.
Gong, G., Rosa-Neto, P., Carbonell, F., Chen, Z.J., He, Y., Evans, A.C., 2009. Age- and gender-related differences in the cortical anatomical network. J. Neurosci. 29, 15684–15693.
Heyer, D.B., Wilbers, R., Galakhova, A.A., Hartsema, E., Braak, S., Hunt, S., Verhoog, M. B., Muijtjens, M.L., et al., 2022. Verbal and general IQ associate with supragranular layer thickness and cell properties of the left temporal cortex. Cereb. Cortex 32, 2343–2357.
Homan, P., Argyelan, M., DeRosse, P., Szeszko, P.R., Gallego, J.A., Hanna, L., Robinson, D.G., Kane, J.M., et al., 2019. Structural similarity networks predict clinical outcome in early-phase psychosis. Neuropsychopharmacology 44, 915–922.
Ingalhalikar, M., Smith, A., Parker, D., Satterthwaite, T.D., Elliott, M.A., Ruparel, K., Hakonarson, H., Gur, R.E., et al., 2013. Sex differences in the structural connectome of the human brain. Proc. Natl. Acad. Sci. 111, 823–828.
Joubert, C., Chainay, H., 2018. Aging brain: the effect of combined cognitive and physical training on cognition as compared to cognitive and physical training alone - a systematic review. Clin. Inter. Aging 13, 1267–1301.
Kent, P., 2017. Fluid intelligence: a brief history. Appl. Neuropsychol. Child 6, 193–203.
Kong, X.Z., Liu, Z., Huang, L., Wang, X., Yang, Z., Zhou, G., Zhen, Z., Liu, J., 2015. Mapping individual brain networks using statistical similarity in regional morphology from MRI. PLoS One 10, e0141840.
Kong, X.Z., Wang, X., Huang, L., Pu, Y., Yang, Z., Dang, X., Zhen, Z., Liu, J., 2014. Measuring individual morphological relationship of cortical regions. J. Neurosci. Methods 237, 103–107.
Li, H., Yang, J., Yin, L., Zhang, H., Zhang, F., Chen, Z., Jia, Z., Gong, Q., 2021. Alteration of single-subject gray matter networks in major depressed patients with suicidality. J. Magn. Reson Imaging 54, 215–224.
Li, J., Seidlitz, J., Suckling, J., Fan, F., Ji, G.J., Meng, Y., Yang, S., Wang, K., et al., 2021. Cortical structural differences in major depressive disorder correlate with cell type-specific transcriptional signatures. Nat. Commun. 12, 1647.
Li, X., Wu, K., Zhang, Y., Kong, L., Bertisch, H., DeLisi, L.E., 2019. Altered topological characteristics of morphological brain network relate to language impairment in high genetic risk subjects and schizophrenia patients. Schizophr. Res 208, 338–343.
Li, Y., Liu, Y., Li, J., Qin, W., Li, K., Yu, C., Jiang, T., 2009. Brain anatomical network and intelligence. PLoS Comput. Biol. 5, e1000395.
Liao, X., Vasilakos, A.V., He, Y., 2017. Small-world human brain networks: perspectives and challenges. Neurosci. Biobehav Rev. 77, 286–300.

Lo, C.Y., He, Y., Lin, C.P., 2011. Graph theoretical analysis of human brain structural networks. Rev. Neurosci. 22, 551–563.
Luo, L., Li, Q., You, W., Wang, Y., Tang, W., Li, B., Yang, Y., Sweeney, J.A., et al., 2021. Altered brain functional network dynamics in obsessive–compulsive disorder. Hum. Brain Mapp. 42, 2061–2076.
Malagurski, B., Liem, F., Oschwald, J., Merillat, S., Jancke, L., 2020. Longitudinal functional brain network reconfiguration in healthy aging. Hum. Brain Mapp. 41, 4829–4845.
Malone, I.B., Leung, K.K., Clegg, S., Barnes, J., Whitwell, J.L., Ashburner, J., Fox, N.C., Ridgway, G.R., 2015. Accurate automatic estimation of total intracranial volume: a nuisance variable with less nuisance. NeuroImage 104, 366–372.
Michael, I.P., Barbey, A.K., 2020. General intelligence in the age of neuroimaging. Trends Neurosci. Educ. 18, 100126.
Morgan, S.E., Seidlitz, J., Whitaker, K.J., Romero-Garcia, R., Clifton, N.E., Scarpazza, C., van Amelsvoort, T., Marcelis, M., et al., 2019. Cortical patterning of abnormal morphometric similarity in psychosis is associated with brain expression of schizophrenia-related genes. Proc. Natl. Acad. Sci. USA 116, 9604–9609.
Nyberg, L., Pudas, S., 2019. Successful memory aging. Annu Rev. Psychol. 70, 219–243.
Parnaudeau, S., Bolkan, S.S., Kellendonk, C., 2018. The mediodorsal thalamus: an essential partner of the prefrontal cortex for cognition. Biol. Psychiatry 83, 648–656.
Seidlitz, J., Vasa, F., Shinn, M., Romero-Garcia, R., Whitaker, K.J., Vertes, P.E., Wagstyl, K., Kirkpatrick Reardon, P., et al., 2018. Morphometric similarity networks detect microscale cortical organization and predict inter-individual cognitive variation. Neuron 97, 231–247 e237.
Shafto, M.A., Tyler, L.K., Dixon, M., Taylor, J.R., Rowe, J.B., Cusack, R., Calder, A.J., Marslen-Wilson, W.D., et al., 2014. The cambridge centre for ageing and neuroscience (Cam-CAN) study protocol: a cross-sectional, lifespan, multidisciplinary examination of healthy cognitive ageing. Bmc Neurol. 14.
Shah, C., Liu, J., Lv, P., Sun, H., Xiao, Y., Liu, J., Zhao, Y., Zhang, W., et al., 2018. Age related changes in topological properties of brain functional network and structural connectivity. Front. Neurosci. 12.
Spreng, R.N., Turner, G.R., 2019. The shifting architecture of cognition and brain function in older adulthood. Perspect. Psychol. Sci. 14, 523–542.
Thomas, C., Ye, F.Q., Irfanoglu, M.O., Modi, P., Saleem, K.S., Leopold, D.A., Pierpaoli, C., 2014. Anatomical accuracy of brain connections derived from diffusion MRI tractography is inherently limited. Proc. Natl. Acad. Sci. 111, 16574–16579.
Tschentscher, N., Mitchell, D., Duncan, J., 2017. Fluid intelligence predicts novel rule implementation in a distributed frontoparietal control network. J. Neurosci. 37, 4841–4847.
Walker, L., Gozzi, M., Lenroot, R., Thurm, A., Behseta, B., Swedo, S., Pierpaoli, C., 2012. Diffusion tensor imaging in young children with autism: biological effects and potential confounds. Biol. Psychiatry 72, 1043–1051.
Wang, H., Jin, X., Zhang, Y., Wang, J., 2016. Single-subject morphological brain networks: connectivity mapping, topological characterization and test-retest reliability. Brain Behav. 6, e00448.
Wang, M., Jiang, J., Yan, Z., Alberts, I., Ge, J., Zhang, H., Zuo, C., Yu, J., et al., 2020. Individual brain metabolic connectome indicator based on Kullback-Leibler divergence similarity estimation predicts progression from mild cognitive impairment to Alzheimer's dementia. Eur. J. Nucl. Med Mol. Imaging 47, 2753–2764.
Wang, Y., Zhang, Y., Zheng, W., Liu, X., Zhao, Z., Li, S., Chen, N., Yang, L., et al., 2022. Age-related differences of cortical topology across the adult lifespan: evidence from a multisite MRI study with 1427 individuals. J. Magn. Reson Imaging.
Weerasekera, A., Ion-Margineanu, A., Green, C., Mody, M., Nolan, G.P., 2023. Predictive models demonstrate age-dependent association of subcortical volumes and cognitive measures. Hum. Brain Mapp. 44, 801–812.
Wei, Y., Scholtens, L.H., Turk, E., van den Heuvel, M.P., 2019. Multiscale examination of cytoarchitectonic similarity and human brain connectivity. Netw. Neurosci. 3, 124–137.
Wolff, M., Vann, S.D., 2019. The cognitive thalamus as a gateway to mental representations. J. Neurosci. 39, 3–14.
Ziegler, G., 2012. Models of the aging brain structure and individual decline. Front. Neuroinformatics 6.
Zuo, N., Salami, A., Liu, H., Yang, Z., Jiang, T., 2020. Functional maintenance in the multiple demand network characterizes superior fluid intelligence in aging. Neurobiol. Aging 85, 145–153.